ELECTRON TRANSPORT AND CHARGE MEMORY EFFECTS IN METAL-DIELECTRIC NANOCOMPOSITES

Final Technical Report
by

S.A.Gurevich, D.A.Zakheim, I.V.Rozhansky, V.A.Zabelin,
V.I.Scopina, I.P.Smirnova, M.M.Kulagina

October 1999

United States Army
EUROPEAN RESEARCH OFFICE OF THE U.S. ARMY
London, England

CONTRACT NUMBER N68171-98-M-5654
R+D no: 8367-EE-01

Contractors name: Prof. S.A.Gurevich
A.F.Ioffe, Physico-Technical Institute
26, Polyteckhnicheskaya, St.Petersburg, 194021, Russia

Approved for Public Release; distribution unlimited

20000118 079

DTIC QUALITY INSPECTED 1

REPORT DOCUMENTATION PAGE

Form Approved
OMB No. 0704-0188

Public reporting burden for this collection of information is estimated to average 1 hour per response, including the time for reviewing instructions, searching existing data sources gathering and maintaining the data needed, and completing and reviewing the collection of information. Send comments regarding this burden estimate or any other aspect of this collection of information, including suggestions for reducing this burden, to Washington Headquarters Services, Directorate for information Operations and Reports, 1215 Jefferson Davis Highway, Suite 1204 Arlington, VA 22202-4302, and to the Office of Management and Budget, Paperwork Reduction Project (0704-0188), Washington, DC 20503.

1. AGENCY USE ONLY (Leave Blank)	2. REPORT DATE	3. REPORT TYPE AND DATES COVERED
	13 Oct 1999	Final report, 24 Jul 1998 - 24 Jul 1999

4. TITLE AND SUBTITLE
ELECTRON TRANSPORT AND CHARGE MEMORY EFFECTS IN METALL-DIELECTRIC NANOCOMPOSITES

5. FUNDING NUMBERS
N68171-98-M-5654 (C)

6. AUTHOR(S)
S.A.Gurevich, D.A.Zakheim, I.V.Rozhansky, V.A.Zabelin, V.I.Scopina, I.P.Smirnova, M.M.Kulagina

7. PERFORMING ORGANIZATION NAME(S) AND ADDRESS(ES)
A.F.Ioffe Physico-Technical Institute
26, Polytekhnicheskaya, St.Petersburg, 194021, Russia

8. PERFORMING ORGANIZATION REPORT NUMBER
4

9. SPONSORING/MONITORING AGENCY NAME(S) AND ADDRESS(ES)
Naval Regional Contracting Center
Detachment London, Block 2, Wing 11
DoE Complex, Eastcode Road Ruislip, MIDDX, UK, HA4 8BS

10. SPONSORING/MONITORING AGENCY REPORT NUMBER

11. SUPPLEMENTARY NOTES

12a. DISTRIBUTION/AVAILABILITY STATEMENT
Public available

12b. DISTRIBUTION CODE

13. ABSTRACT (Maximum 200 words)
The purpose of this work is to study the mesoscopic limits of conductivity in granulated materials like metal-dielectric nanocomposites and to reveal the major design features of mesoscopic transistor (and charge memory device) made of these materials. Thin composite $Cu:SiO_2$ films containing 2-3 nm Cu granules were fabricated and temperature dependencies of conductivity were measured (in dielectric regime) as function of Cu content and the sample size. The experimental results are analyzed using newly developed numerical model of conductivity which deals with the network of tunneling resistance between randomly arranged small metallic balls, accounts for Coulomb interaction between charged balls, and essentially incorporates screening effects. It is found that the experimental conductivity of all the samples follows the universal "$T^{-1/2}$" law at low temperatures (T<100K) which is treated as the manifestation of Coulomb gap in the density of states of composite material. Both simulations and experiment show that the mesoscopic limit of the composite sample size is about 20-30 nm at T~300K (and ~50 nm at 30K). We argue that with such small samples it should be possible to implement the room temperature single-electron transistor device by applying the electric field perpendicular to the current chain.

14. SUBJECT ITEMS
composite material, granulated metal, hopping conductivity, Coulomb interaction mesoscopic interaction

15. NUMBER OF PAGES
28

16. PRICE CODE

17. SECURITY CLASSIFICATION OF REPORT	18. SECURITY CLASSIFICATION OF THIS PAGE	19. SECURITY CLASSIFICATION OF ABSTRACT	20. LIMITATION OF ABSTRACT
UNCLASSIFIED	UNCLASSIFIED	UNCLASSIFIED	UL

Abstract.

The purpose of this work is to study the mesoscopic limits of conductivity in granulated materials like metal-dielectric nanocomposites and to reveal the major design features of mesoscopic transistor (and charge memory device) made of these materials. Thin composite $Cu:SiO_2$ films containing 2-3 nm Cu granules were fabricated and temperature dependencies of conductivity were measured (in dielectric regime) as function of Cu content and the sample size. The experimental results are analyzed using newly developed numerical model of conductivity which deals with the network of tunneling resistance between randomly arranged small metallic balls, accounts for Coulomb interaction between charged balls, and essentially incorporates screening effects. It is found that the experimental conductivity of all the samples follows the universal "$T^{-1/2}$" law at low temperatures (T<100K) which is treated as the manifestation of Coulomb gap in the density of states of composite material. Both simulations and experiment show that the mesoscopic limit of the composite sample size is about 20-30 nm at T~300K (and ~50 nm at 30K). We argue that with such small samples it should be possible to implement the room temperature single-electron transistor device by applying the electric field perpendicular to the current chain.

List of keywords.

Composite material, granulated metal, hopping conductivity, Coulomb interaction, mesoscopic effects.

Table of contents.

1. Background and statement of the work 2
2. Fabrication and structure studies of composite $Cu:SiO_2$ films 4
3. Conductivity of bulk and sub-micron composite conductors 9
4. Development of the model of conductivity 13
5. Results and discussion 21
6. Conclusions and recommendations 23
7. Literature cited 24

1. Background and statement of the work.

The effect of macroscopic charge quantization [1], which has been under extensive study during the last decade, can be observed, in general, in the structures containing small metallic particles separated by tunnel barriers. This effect shows up when the size of the particles is sufficiently small such that their charging energy $E_c=e^2/2C$ (C is the particle capacitance) exceeds thermal noise under the experimental conditions, $E_c \gg kT$. The other requirement is that the particle should have weak coupling to the environment. In other words, the characteristic tunnel resistance in the system should be higher than the resistance quantum $R_q=\hbar/e^2$=4.1 kΩ. The major manifestation of macroscopic charge quantization is so called Coulomb blockade which appears as the threshold voltage needed to push the current through the system of small particle separated from the contact leads by two tunnel barriers. Adding the third gate electrode allows to control the threshold voltage thus resulting in the single-electron transistor (SET) [2]. In some sense, SET is an ultimate transistor since its conducting state is controlled by only one electron.

Considering the possibility for practical realization of SET (and similar devices like single-electron memory cell), following major problems appear. First, the conducting particle should be indeed very small. If, for example, the structure is fabricated by means of e-beam lithography, the reasonable minimum size of the feature is about hundred nanometers, leading to the charging energy $E_c \approx 10$K (and tunnel resistance $R \approx 100$ kΩ). In this case the charge quantization can be observed only at temperatures below 1K. One possible way to increase the operating temperature could be to assemble the desired structure from nm-size metallic particles produced, for example, by STM-related technology [3]. In this case the charging energy is $E_c \approx 10^3$K which allows to operate at room temperature. However, for all kinds of "artificially arranged" structures severe problem is associated with dimension tolerance. In fact, the characteristics of SETs are known to be rather sensitive to the central particle capacitance and the tunnel barrier resistance which impose hard requirements to the accuracy of controlling the corresponding structure parameters. To cope with this problem it was suggested [4] to adjust the position of metallic island in SET structure *in situ* by using STM tip but obviously this approach is very far from any practical fabrication process. Finally, the fractional charge residing at small conducting particles [5] constitute very serious problem for "hand-made" single-electron device structures.

On the other hand it was suggested [6] that useful single-electron devices, capable of operating at elevated temperature, can be made of *randomly arranged* granulated materials in which nanometer-size conducting particles are naturally formed at the stage of material fabrication. Contrary to the ordered structures, random materials are characterized by particle size distribution function $F(d)$ of finite width and by certain distribution of mean minimum distances between nearest neighbors $H(s)$ (d is the particle diameter and s is the inter-particle distance). The major idea is that in sufficiently small disordered conductors (presumably having the size $L \sim 10(d+s)$), the current should flow through one self-selected chain of particles, along which the tunneling probability is the highest. According to [7] this chain will be chosen, among other possible paths, in such a way that along the chain the tunneling distances are minimum and approximately equal. Also, the sizes of particles in the chain should be approximately equal. The formation of such chains and related incoherent mesoscopic effects were analyzed in detail in [7]. The important statement is that the current through this chain is due to single electron tunneling [6]. This current increases sharply above the threshold voltage (similar to Coulomb blockade), the threshold being about 10 E_c (or about 1 V) in the considered example. At the same time the value of the threshold should be quite reproducible [6] because of the chain selection mechanism. By implementing the outer

gate electrode it is possible to control this threshold. The important aspect of this proposition is that for the fabrication of such SET devices e-beam lithography can be used for writing the contact leads and for outlining the shape of conductor but not for patterning very small conducting islands. This strongly simplifies the device fabrication.

Perhaps, the first step toward using disordered materials for single-electron devices has been made in [8]. In this work room temperature operating single electron memory cell was demonstrated, made on poly-silicon film annealed to create nanometer Si inclusions. Another prototype of such devices was reported in [9]. In this work the Coulomb blockade was observed at 77 K in the structure containing 2-3 nm metallic islands deposited (and randomly located) in the gap between sub-micron contact leads. The other material approach is to use metal-dielectric composites which are known to contain nm-size metallic inclusions randomly spread in dielectric matrix [10]. In this kind of material the appearance of charge quantization was demonstrated at room temperature [11]. Regarding this, the main objective of the present work is to study the possibility to create room temperature single-electron devices on the basis of metal-dielectric composites. Our approach is that the conductivity of metal-dielectric composites is studied in close relation with detail understanding of the material microstructure.

Besides of practical meaning, the problem under consideration is also of general interest because the conductivity of disordered granulated materials, especially in mesoscopic regime, is as yet imperfectly understood. Contrary to orthodox approach [1] commonly used to describe the behavior of single-electron devices with pre-defined parameters, the characteristics of randomly arranged structures must be analyzed by means of statistical methods. Starting from the early papers [10, 12], a number of studies have been carried out in this direction. The important results were obtained considering closely related problem of hopping conductivity of doped semiconductors [13]. In particular, it was found that Coulomb interaction between randomly located charged impurity centers results in Coulomb gap in one-particle density of states near the Fermi level [14]. Later on, these results were transferred to the analysis of the conductivity of granulated metals in the dielectric regime, where the widely observed $-ln\sigma \sim T^{1/2}$ law of conductivity has been interpreted as a manifestation of the Coulomb gap [15]. Recently, the detail studies of the ground state of the granulated metals [16] and of the Coulomb gap in the density of states [17] has been undertaken. A lot of attention was paid also to the origin of random potential at the grains [16], which is an important source of system disorder. However, to the best of our knowledge, these results have not been applied to calculate the conductivity of granulated metals. Perhaps, the first attempt to do this has been undertaken in course of the present work.

As the above discussion was concerned with the conductivity of granulated metals (and composites) in bulk, the mesoscopic conductivity of small conductors constitute even more difficult problem. Here, individual random realizations of the particle positions in the conductor should be considered. Then, taking into account that the system is in thermal equilibrium, the statistics should be included to describe the random potential, the filling of excited states, and the tunneling probabilities between the particles. We have tried to develop such model in order to clarify the size limit for the mesoscopic conductivity and to study the properties of conducting chains formed in this regime. It is to note that besides [6], the formation of current punchers (chains) in granulated metal has been analyzed in [18] by means of numerical simulation but this model is too simplified to get the practical results. In our model the formation of mesoscopic current paths has also been confirmed. Practical recommendations are given how to control these current chains in order to realize the transistor functions.

2. Fabrication and structure studies of composite $Cu:SiO_2$ films.

2.1. The film deposition technique.

Composite $Cu:SiO_2$ films which are the main object of studies in this work were fabricated using the well known method of co-sputtering [10]. In our experiments we used Alcatel SCM 450 machine equipped with two magnetron sources: one with metallic Cu target and the other with pure quartz. These two magnetrons were operating simultaneously with dc bias supplied to the Cu source and RF power delivered to the SiO_2 source. The substrate holder has been rotating over the magnetrons so that in each path less than one monolayer of Cu and SiO_2 is deposited. In the experiments the rate of Cu deposition was kept constant at about 0.4 nm min^{-1} and the rate of SiO_2 deposition was varied in the range 0.6 - 1.5 nm min^{-1}. This allowed to vary the average Cu content in the film from 17 to 35 volume percent. The films, typically about 100 nm thick, were deposited on thermally oxidized Si substrates (the thickness of oxide layer was 300-500 nm). During the deposition the substrate was kept at the room temperature. Using X-ray microanalysis carefully calibrated for present purposes the Cu content in the fabricated films was measured with the accuracy of about 1 %.

Most of the conductivity studies were performed on as-made films, while some of the structure studies has been carried out using the films additionally annealed in pure hydrogen atmosphere. Regarding the deposition process one could expect that the structure of as-made films will be equal apportionment of Cu in SiO_2. However, according to [10], it was found that in as-made films the Cu atoms are segregated in small clusters. In the annealed films, depending on the temperature and time of annealing, the cluster size is bigger. The origin of Cu segregation and the details of microstructure of the fabricated $Cu:SiO_2$ films are discussed below.

2.2 TEM and X-ray scattering studies of the film structure.

Fig. 1 represents TEM images of as-made films with Cu content 21 % and 27 % (the reference image taken from pure SiO_2 film is also displayed for comparison). These figures show that as-made films contain Cu clusters whose diameter is typically about

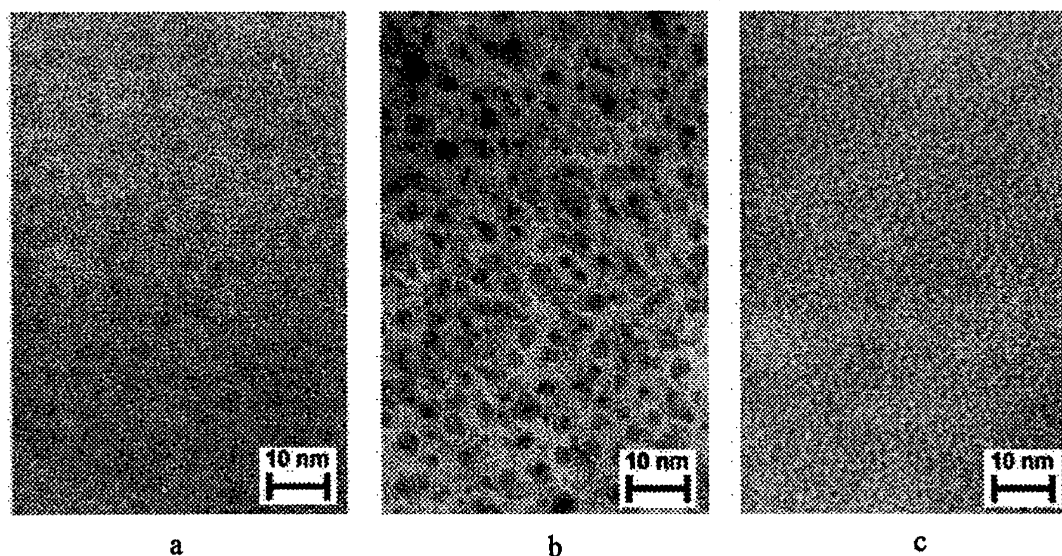

Fig. 1. TEM images of as-made $Cu:SiO_2$ films with Cu concentration 21 vol.% (a), 27 vol.% (b) and pure SiO_2 film (c).

3 nm. Fig. 1 shows also that the size of the clusters as well as their density depend on the average Cu content. In spite the resolution of our TEM is limited, close inspection of these images allows to conclude that the structure of the Cu clusters is rather complex. The clusters seem to be not metallic balls but rather "clouds" of Cu atoms with dense nuclei in the center.

It would be reasonable to suggest that Cu atom segregation observed in as-made films originates from local surface heating which occurs during the film deposition due to surface bombardment by impacting atoms (molecules). Taking into account that in the process of magnetron sputtering the characteristic energy of impacting atoms is about 10 eV, the overheating of the film volume of the cluster size can be easily estimated to be about 100 K. We believe that such overheating may activate local diffusion of Cu in SiO_2 matrix. To some extent this assumption is confirmed by the results of our experiments in which the film conductivity was found to change after short sample annealing at the temperatures exceeding 400 K.

Further study of the film structure has been performed by means of small-angle X-ray scattering spectroscopy. The experimental scattering patterns, i.e. the intensity vs. parameter $s=(2\pi/\lambda)\sin\alpha$ (λ is the X-ray wavelength and α is the angle of scattering) are shown in Fig. 2. Characteristic for the pattern taken from as-made film is the presence of a single peak positioned at certain small angle (see Fig. 2a). For the Cu concentration equal to 30 vol.% this peak is found at $s\approx 0.15$ Å^{-1} or at $\alpha\approx 2°$. The other feature is a plateau presented at smaller angles. For the annealed film (800 °C, 30 s) with the same Cu content the scattering pattern is different (Fig. 2b): it contains strong peak positioned at $s\approx 0.03$ and the weak shoulder extended up to $s\approx 0.2$. To understand the above features the numerical simulations of small-angle X-ray scattering has been performed.

In our model we start with the well known expression for the scattering amplitude of a single ball which is given, for example, in [19]:

$$F(sR)=3(sR)^{-3}[\sin(sR)-sR\cos(sR)]. \qquad (2.1)$$

Here R is the ball radius and s is the scattering parameter denoted above. Then, the intensity of scattering $I(s)$ which results from the ensemble of the balls is found by summing single-ball scattering amplitudes:

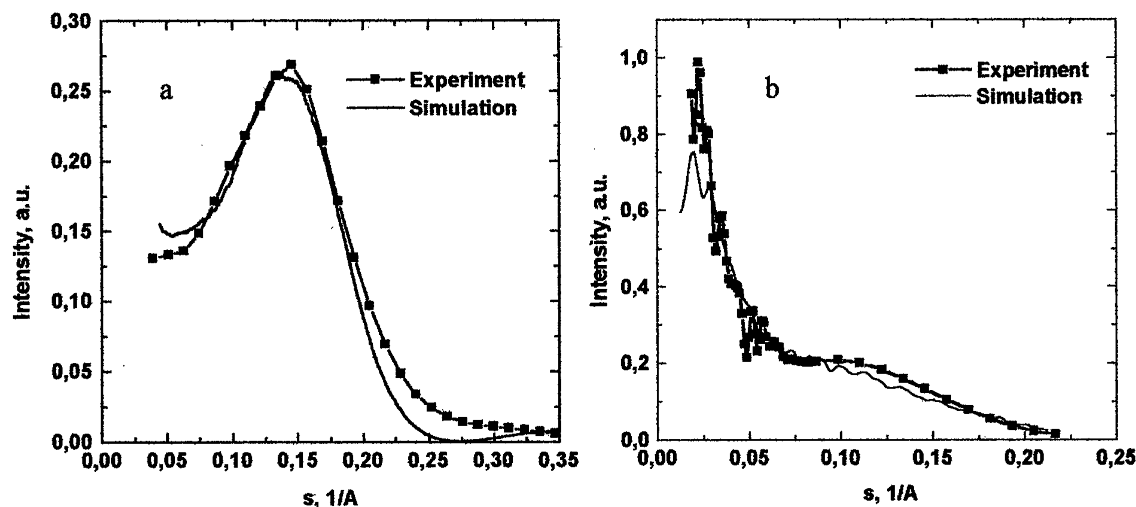

Fig.2. Small angle X-ray scattering intensity for as-made (a) and annealed (b) composite films with Cu concentration 30 vol.%.

$$I(s) = F(sR)^2 \left| \sum_j e^{ikr_j} / r_j \right|^2 . \quad (2.2)$$

In this expression r_j are the coordinates of the scattering centers. The essential feature of this approach is that it takes into account the interference effects which are expected to be of major importance when, as in our case, the concentration of scattering centers is high enough.

In simulation, the first step is to distribute randomly the balls of given radius R within the sample cube (or parallelepiped). Doing this the number of balls was chosen so that the volume part equipped with the balls is equal to some predefined value. Then, the scattering intensity is calculated according to (2.2). Obviously, such simulation procedure should be rather time consuming if the number of the balls is large. In practice, the number of balls in simulation could be much smaller than the number of clusters in the experimental sample. This is the limitation which may create difficulty when describing the scattering intensity at very small angles (corresponding to the size of sample parallelepiped). To overcome this difficulty we have averaged the simulated intensity over a number of random realizations, choosing the optimal shape of sample parallelepiped in one realization.

In Figs. 2a,b solid lines represent the simulated small-angle scattering intensities. As one can see in this figure there is very close agreement between experimental and simulated curves. In simulation of the scattering pattern for as-made film the best fit of calculated curve has been obtained assuming the ball diameter is equal to 3 nm, which is in good agreement with TEM data. Our analysis shows that the presence of the peak and plateau in Fig. 2a is the direct result of the interference of the scattering fields produced by the individual balls (clusters). This statement becomes specifically clear if one will note that the single-ball scattering intensity given by (2.1) essentially has a peak at zero angle. As for the annealed film, the best fit of simulated curve in Fig. 2b has been obtained assuming the scattering is produced by two groups of balls: one 3 nm in diameter (80% of total number of balls) and the other having the size of 12 nm (20% of balls). Qualitatively, this assumption is confirmed by TEM images of annealed films where rather broad dispersion of cluster size can be directly observed.

According to the theory of phase decomposition [20] the above results can be understood as follows. In as-made films the nucleation process has only came about which resulted in formation of small Cu clusters, all having nearly the same size. During the annealing the coalescence starts which gives certain amount of bigger clusters. The essential general feature of phase decomposition process is the presence free-standing add-atoms in the matrix until the aging time is not too long (or the temperature is not too high). Thus, in our case one could expect the presence of free-standing Cu atoms in SiO_2 matrix. It would be important to know the fraction of free-standing Cu atoms in our films because this may be the significant parameter related to the transport properties. However, we found that neither TEM nor small-angle X-ray scattering can be used to evaluate this structure parameter. Moreover, it was found that in case of high Cu content both TEM and X-ray scattering do not permit to get the reliable data on cluster size distribution function and inter-cluster distances. To gain the understanding of the microstructure of composite films direct simulation of the cluster growth process has been performed.

2.3 Computer simulation of the cluster formation process.

The developed model [21] deals with bulk diffusion of copper atoms in the lattice matrix representing SiO_2 host material. Initially, the copper atoms were placed at random at the sites of this matrix so that the total number of atoms corresponds to a given average Cu concentration in the film (the size of the lattice sell is 0.27 nm which corresponds to the Cu

lattice parameter). Then, it is assumed that diffusing from one site to the other copper atoms interact mainly with nearest copper atoms standing in the first and the second coordinate spheres. It is assumed also that Cu-Cu interaction is stronger than Cu-SiO_2 interaction. Changing its position each Cu atom prefer to move toward the state with larger number of Cu neighbors which is energetically more favorable.

It is to note that this approach based on consideration of bulk Cu diffusion is not absolute. Its insufficiency is that the surface diffusion of Cu atoms is ignored. In fact, the surface diffusion may play role in the formation of Cu clusters during the film deposition by co-sputtering. However, the inclusion of both surface and bulk diffusion in the model will strongly complicate the simulation. That is why in the present simplified model only bulk diffusion is considered.

The probability for the Cu atom to occupy a site in the lattice is given by:

$$P \propto \exp\left(\frac{E_b}{kT}\right), \quad (2.3)$$

where E_b is the binding energy. The binding energy E_b of copper atom can be expressed as:

$$E_b = n_{1Cu}E_{1Cu-Cu} + n_{1SiO_2}E_{1Cu-SiO_2} + n_{2Cu}E_{2Cu-Cu} + n_{2SiO_2}E_{2Cu-Cu} \ . \quad (2.4)$$

Here n_{1Cu}, n_{2Cu} and n_{1SiO2} and n_{2SiO2} are the numbers of copper and SiO_2 neighbors in the first and the second coordinate spheres, E_{1Cu-Cu} and E_{2Cu-Cu} are the binding energies of Cu-Cu bonds in the first and the second coordinate spheres, and $E_{1Cu-SiO2}$, $E_{2Cu-SiO2}$ are the binding energies of Cu-SiO_2 bonds. Since the total number of atoms in coordinate spheres is fixed (this number depends on the lattice type and for the cubic lattice it is 6 in the first and 12 in the second coordinate sphere) expression (2.4) can be rewritten as:

$$E_b = n_{1Cu}\left(E_{1Cu-Cu} - E_{1Cu-SiO_2}\right) + n_{2Cu}\left(E_{2Cu-Cu} - E_{2Cu-SiO_2}\right) + E_0, \quad (2.5)$$

where E_0 is the binding energy of solitary copper atom surrounded by SiO_2 molecules. As follows from (2.5) the important parameters determining the cluster growth are the difference between the energies of Cu-Cu and Cu-SiO_2 bonds. The reasonable assumption is that the main part of the binding energy is associated with the first coordinate sphere bonds so that $E_1 = E_{1Cu-Cu} - E_{1Cu-SiO2} > E_2 = E_{2Cu-Cu} - E_{2Cu-SiO2}$.

In simulation the copper atom is first randomly selected and its binding energy in initial and each of accessible neighboring sites is determined using expression (2.5). Since the atom can jump only to the site unoccupied by Cu atoms in the first or the second coordinate sphere, the maximum number of possible target positions is limited. In the cubic lattice this number is 18. Then, the relative probabilities of occupation of each accessible sites are calculated using (2.3) and the atom is moved to a new position according to these probability values. Jumping to more preferable site the atom can form new small cluster or join already existing bigger one. (In general, the back way is also possible: the atom can outstand their neighbors but the probability of this process is exponentially small.) After moving the first atom, its position is fixed, the next atom is randomly selected and the procedure repeats.

It has been found that in case E_1 is less than about 0.5 kT (T=300 K), diffusion does not lead to the formation of clusters. Rather, only free standing copper atoms or very small conglomerates of atoms can be found in the matrix volume even after sufficiently large number of jumps. Contrary to this, if $E_1 > 0.5\ kT$, copper atoms easily form clusters and the part of free standing copper atoms shortly becomes to be small.

As an example, Fig. 3 shows simulated TEM pattern of the structure formed after $6 \cdot 10^8$ atom jumps in the lattice. The initial Cu content was taken to be 27 volume percent. The

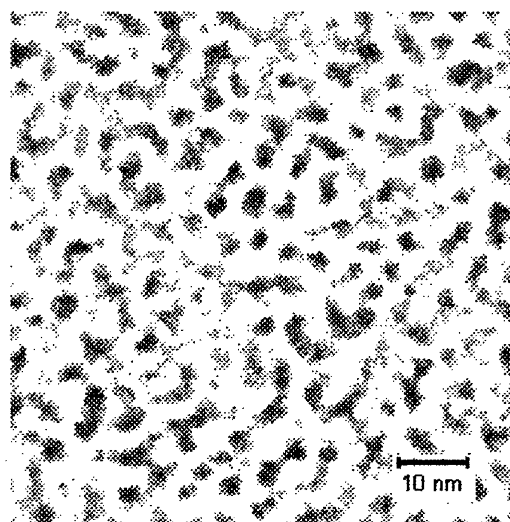

Fig.3. Simulated TEM image.

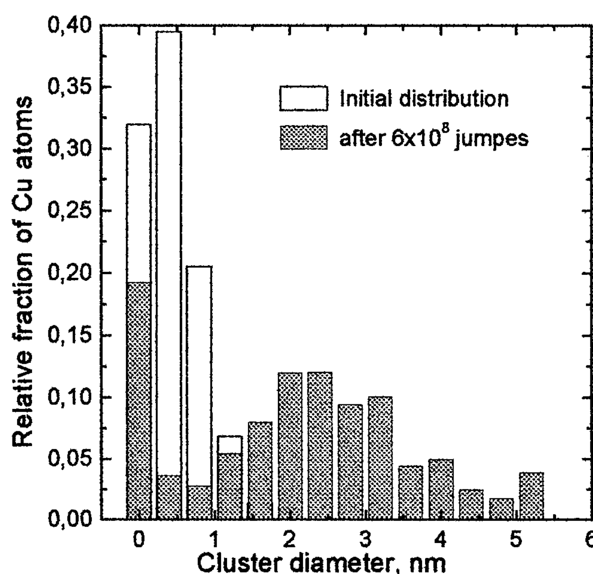

Fig.4. Simulated cluster size distribution function.

pattern shown in this figure has been obtained by superimposition of 10 successive molecular layers taken from the lattice matrix. The simulation was performed in the matrix of the size 200x200x200 sites with E_1 =0.6 kT and E_2 = 0.15 kT. These values correspond to the difference between complimentary binding energy of Cu atom surrounded by only the copper atoms and the binding energy of solitary copper atom surrounded by SiO_2 molecules equal to about 5.5 kT.

Regarding Fig. 3 one can see that the structure obtained by direct diffusion simulation is in excellent agreement with that observed in the experiment (see Fig. 1). The mean size of the clusters in the simulated pattern is about 3 nm, as in the experimental TEM image. It is interesting to note that even the fine details of simulated and experimental structures are similar. In particular, the simulated clusters are also the "clouds" of atoms, sometimes having the dense nuclei in the center. This suggests that our model is capable for the right description of the cluster growth process and that the parameter values used in simulation are properly chosen.

Fig. 4 shows the fraction of Cu atoms in the cluster plotted against the cluster size (the size distribution function) extracted from the simulated Cu atom distribution in 200x200x200 sites matrix. In this figure the open columns represent the initial random distribution of Cu atoms. Since the copper content is high (27 vol.% of Cu), in this initial distribution the free-standing Cu atoms, Cu dimers and even trimers can be found. Contrary to this, dark columns represent the Cu atoms distribution appeared after $6 \cdot 10^8$ atom jumps. The presence of Cu clusters with the mean diameter of about 3 nm is clearly seen in this distribution. It can be seen also in this figure that about 10 volume percent of Cu atoms still remain to be in atomic and dimer states. This result supports the above mentioned statement of the theory of phase decomposition.

As a supplement to Fig. 4 the diagram presented in Fig. 5 shows the distribution of the inter-cluster distances throughout the simulated structure. In this diagram the height of each column indicates the mean minimum inter-cluster distance, whereas the position of the column on the horizontal plane shows the size of primer cluster and the size of neighboring cluster, the distance to which is to be determined. The interesting result which can be seen in

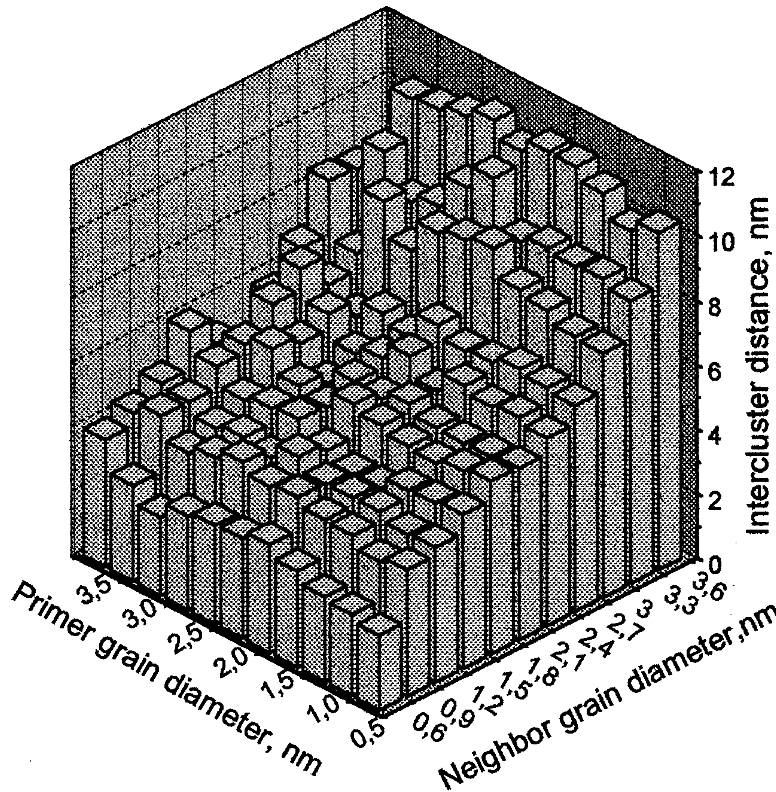

Fig.5. Distribution of the inter-cluster distances.

this plot is that the inter-cluster separation is rather weak function of primer cluster size. The other feature is monotonous growth of inter-cluster distances with increasing the neighboring cluster size. We would like to note that this result is in agreement with the assumption of Abeles et.al. [10] who claimed that in the composite material similar to ours the ratio of inter-cluster distance to cluster size is constant over the sample volume.

The above results on the microstructure of composite films were used as a reference when considering their electric transport properties.

3. Conductivity of bulk and sub-micron composite conductors.

3.1 Experimental samples.

Two types of experimental samples, "bulk" and sub-micron, have been fabricated to measure the conductivity of Cu:SiO_2 composites. Bulk samples were fabricated by using common optical lithography processing. First, the islands of composite film were formed on oxidized Si substrate by lift-off technique. Then, the lateral contacts at the top of the film islands were formed by lift-off technique, so that within the sample the gap between contacts varied from 5 μm to 200 μm (the width of all the conductors was equal to 400 μm). In the sample fabrication the contact deposition was the subject of special attention. In order to have reproducible results, before the contact deposition the film surface was pre-etched by Ar ions. This allowed to remove possible surface contamination and oxide layers. As for the contact metal, Cr was chosen since it has good adhesion and, what is most important, provides ohmic contact to the composite film. Ohmic behavior of the contacts has been carefully checked by

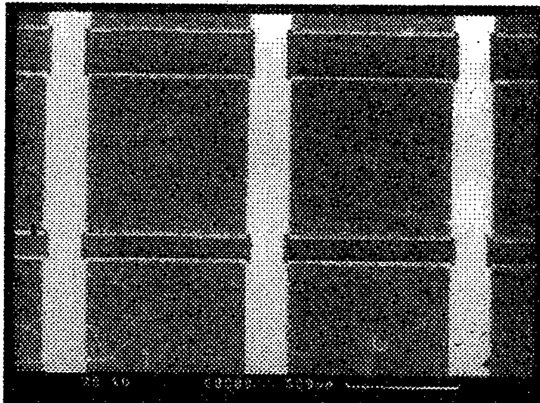

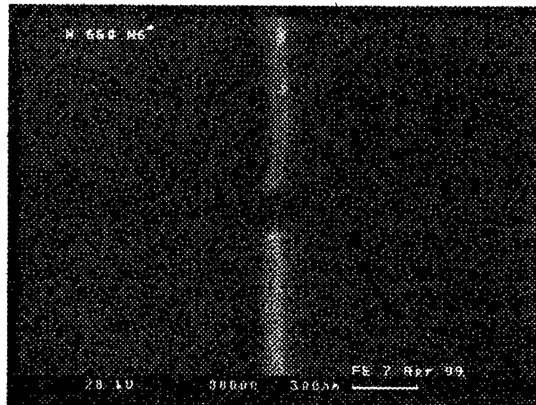

Fig.6. SEM top view of the "bulk" sample.

Fig.7. SEM top view of sub-micron sample

examining the sample I-V curves. The thickness of the Cr layer was typically 50 nm and for easy contacting the sample Cr was covered by about 100 nm thick layer of gold. Fig. 6 shows the SEM top view of the fabricated "bulk" samples.

In general terms, the fabrication of sub-micron samples was similar except the lateral contacts at the top of composite film islands were formed by means of e-beam lithography. For e-beam writing JXM 50A (Jeol) microscope was used equipped with lithographic unit. The photograph of the fabricated sample is shown in Fig. 7. As can be seen in this figure, the width of the contact stripes is somewhat less than 100 nm and the gap between them is about 150 nm. It was found that the major limiting factor preventing from further reduction of the pattern size is, in our case, the size of the e-beam spot. Perhaps, more careful procedure for the beam focusing should be introduced to diminish the stripe width (and the gap).

In all the experiments the thickness of the composite film was typically 150 nm and the copper content in SiO_2 was selected in the range 15-35 volume percent. At lower copper concentration (or smaller film thickness) the conductivity of the samples, especially of sub-micron ones, was too small to be accurately measured. On the other hand, at higher copper concentrations the film conductivity approaches the percolation threshold but this regime is beyond the scope of studies in this work.

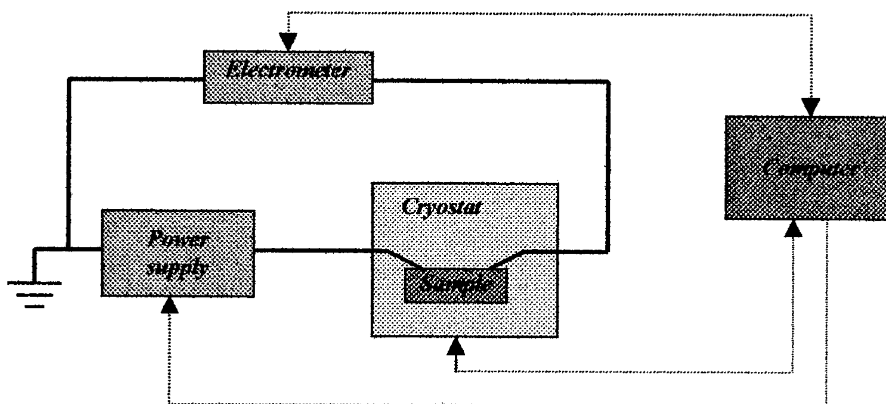

Fig.8. Experimental setup.

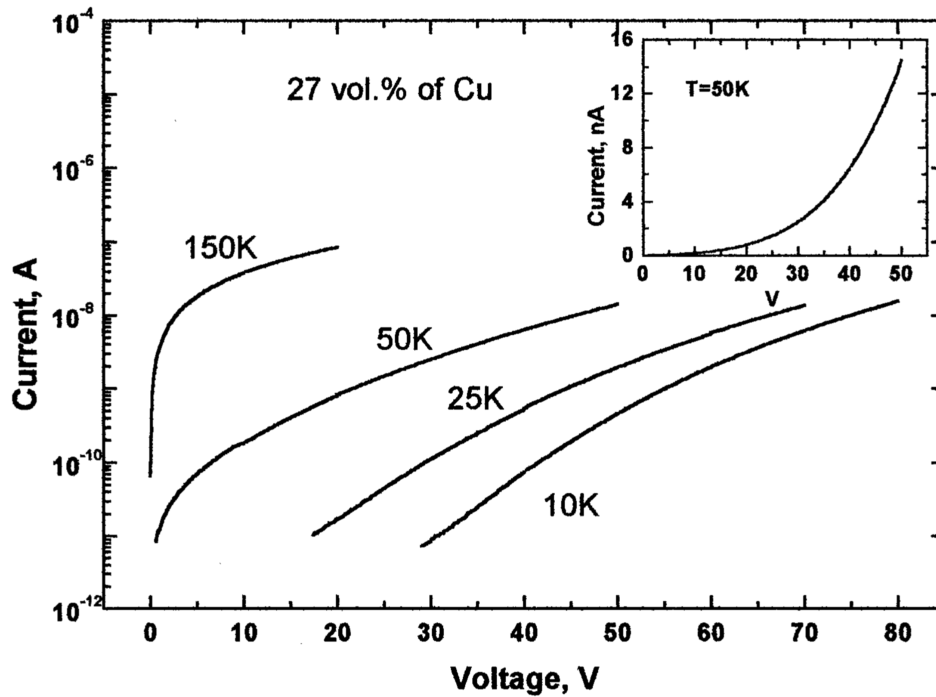

Fig. 9. The experimental I-V curves of bulk composite sample.

3.2 Conductivity measurements in Cu:SiO_2 composites.

The conductivity of the samples was measured using the experimental setup which is shown schematically in Fig. 8. The samples were placed in closed circle helium cryostat (Oxford 450) which allowed to measure the conductivity in the temperature range 20-300 K. The current was measured by sensitive electrometer (B7-49) with the detection limit

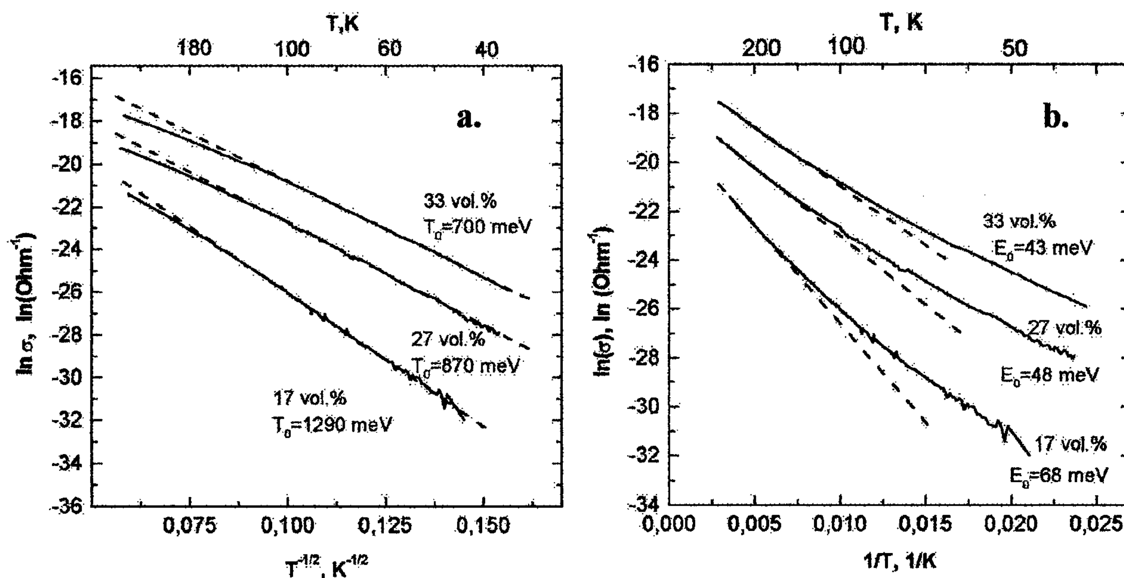

Fig. 10. Experimental temperature dependencies of bulk sample conductivity.

~10^{-13} A. All the measurements were computer controlled.

Fig.9 shows typical I-V curves of bulk sample (27 vol.% of Cu, 5μm gap) taken at different temperatures. All curves are linear at voltages below certain threshold. The value of threshold voltage was found to be strongly temperature dependent. While at room temperature the I-V curves are linear within the whole range of applied voltages, at low temperatures they are mostly exponential-like with short linear part at low voltages. As an example, the I-V curve taken at 50K is shown in the inset in linear scale. The threshold voltage was also proved to be dependent on the Cu content. At higher Cu content the nonlinear character of I-V curves shows up at lower voltages.

Shown in Fig. 10a are the temperature dependencies of low-field conductivity of bulk samples with the copper concentrations 17, 27, and 33 volume percent. Here, the logarithm of conductivity is plotted vs. reversed square root of the temperature (the bottom axis). The main feature of this plot is that for all the concentrations under consideration the conductivity closely follows $\sigma \sim \exp[-(T_0/T)^{-1/2}]$ law at low temperatures. However, at high temperatures the deviation from this law to higher power of T can also be observed. The starting point of this deviation depends on the copper content, and for the sample with 33% of Cu it is at about 100 K. Also, the slope parameter T_0 is found to diminish with increasing the copper concentration. It would be instructive to observe the above dependencies plotted in the form $\sigma \sim \exp[-E_0/kT]$ (Fig. 10b). As can be seen in this figure at high temperatures the conductivity is of activation type with the activation energy E_0 depending on Cu content.

The I-V curves and temperature dependencies of conductivity have also been measured on sub-micron samples. Fig.11 shows the I-V curves of such sample with 27 vol.% of Cu in the film taken at different temperatures. Comparing the results shown in Fig.9 and Fig.11 one can see that the general behavior of I-V characteristics is similar except of different voltage and current scales. In case of sub-micron samples the value of threshold voltages separating linear and nonlinear regimes are about 10 times lower than for bulk samples. This fact is in some contradiction with the assumption that the threshold electric field should be the same in these two kinds of samples (note that the gap width in sub-micron samples is about 50 times smaller). The reason for this discrepancy may be that the effective

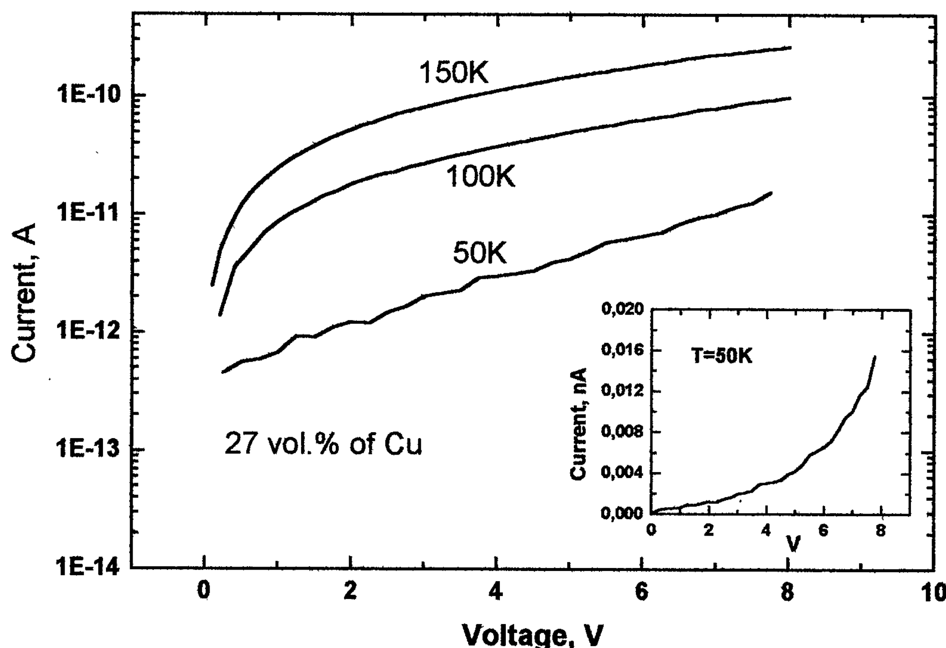

Fig.11. The experimental I-V curves of sub-micron sample.

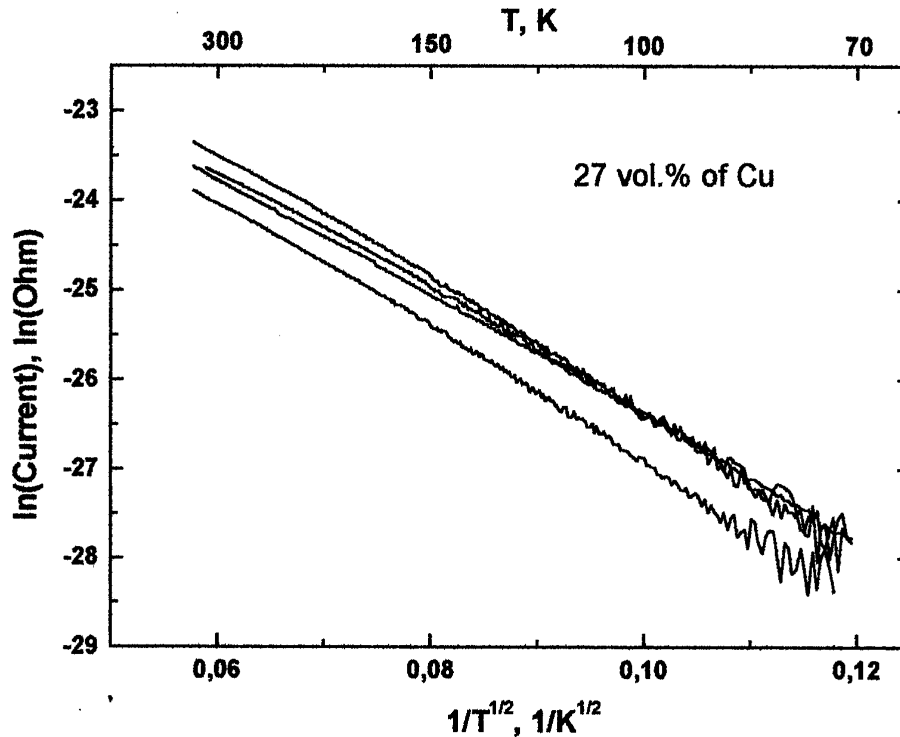

Fig.12. Experimental temperature dependencies of sub-micron samples conductivity.

size of the gap in sub-micron samples is larger than geometrical one due to the current spreading. Also, this discrepancy may be associated with the impact of contacts. If there is a depleted region near the contacts and the size of this region is comparable to or larger than the gap between contacts, the contacts may limit the current at high voltages. Presumably, this is not the case for bulk samples.

Temperature dependencies of conductivity of several sub-micron samples are presented in Fig.12. All these curves follow the $T^{-1/2}$ law with some spread of the slopes. This spread is an important feature which will be discussed later in comparison with the results of simulations.

4. Development of the model of conductivity.

In order to perform the quantitative analysis of obtained experimental data and understand better the nature of composite material electrical properties we have developed the detailed numerical model of composite material conductivity.

In our numerical model the granular medium is considered as a collection of metallic spheres which have a fixed radius r and are randomly arranged in a fixed volume. The parameter of such an arrangement is the minimum admissible distance Δ_{min} between neighboring spheres. The following method was used to implement the quasirandom arrangement numerically: Initially the spheres were arranged in a regular cubic lattice, after which an initial velocity was assigned to each sphere according to a random law and the motion of all spheres was calculated with their collisions taken into account. The effective radius of the spheres was taken to be $r^{eff}=r+\Delta_{min}/2$. This guaranteed that the distance between the spheres cannot be less than Δ_{min}. In addition, all collisions were assumed to be completely inelastic, i.e., after each collision the velocity of a sphere was once again considered to be

random. The calculation was terminated after each sphere had undergone a large number (several tens) of collisions, and the arrangement obtained was used as a random realization.

4.1. Calculations of the capacitance matrix.

First of all, it is necessary to determine the ground state of a system of metallic particles and to find the spectrum of its excitations involving transitions of electrons between particles. In turn, this requires the matrix C_{ij} of the capacitance and electrostatic inductance coefficients which relates the energy of the system with its charge state:

$$E = \frac{1}{2}\sum_{i,j} C_{ij}^{-1} Q_i Q_j \,. \qquad (4.1)$$

To calculate the diagonal elements of this matrix (the capacitance coefficients) it is sufficient to calculate the charging energy E_{ci} of each particle in a neutral environment, while the off-diagonal elements (the electrostatic coefficients) are determined from the charging energy V_{ij} of a pair of particles in a neutral environment.

In existing theoretical works the mean-field approximation is ordinarily used to estimate the energies E_{ci} and V_{ij}, or the Coulomb interaction is calculated using formulas for point charges and an effective permittivity. However, neither approximation is substantiated, specifically, the concept of effective permittivity itself is applicable only at distances that are large compared with the scale of nonuniformity of the medium. Moreover, both approaches completely ignore the rms deviation of E_{ci} and V_{ij} due to the randomness of the relative arrangement of the metallic particles in the medium.

We suggest the procedure for more accurate calculation of the electrostatic interaction energies in a system of charged metallic particles in the case when the particle sizes are comparable to the interparticle distances, and therefore the particles cannot be regarded as point charges [22].

In the zeroth approximation the charging energy of a metallic sphere is $E_{c0}=Q^2/2\varepsilon r$, where Q is the charge of the sphere, and ε is the permittivity of the surrounding medium. The coefficient $1/\varepsilon r$ is the reciprocal C^{-1} of the electric capacitance of the sphere. In first order of the dipole expansion, the polarization of neutral spheres surrounding a given charged sphere must be taken into account. For this, we shall consider first the existing analytical solution of the problem of the interaction energy of two metallic spheres, of which one is charged to a charge Q while the other is neutral. To a first approximation we shall assume that the charge distribution in the charged sphere is uniform, and we shall construct the polarization of the neutral sphere by the method of images (Fig. 13a). We shall calculate the electrostatic energy of such a system as the energy of the electric field in all space outside the spheres:

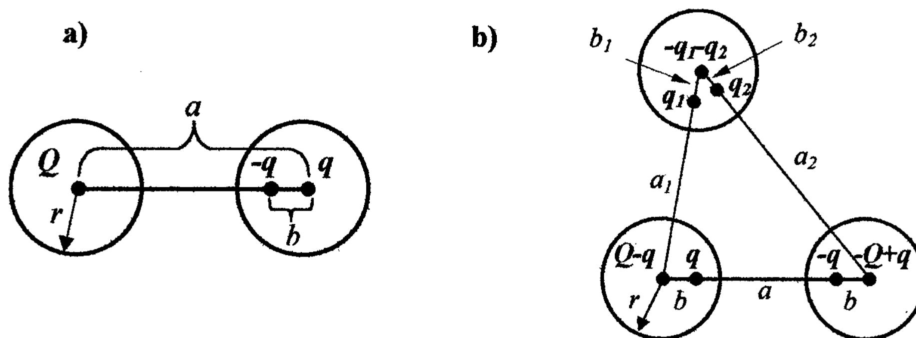

Fig.13. Method of images for two (a) and three (b) spheres: $b=r^2/a$, $b_1=r^2/a_1$, $b_2=r^2/a_2$, $q=Qb/r$, $q_1=Qb_1/r$, and $q_2=Qb_2/r$.

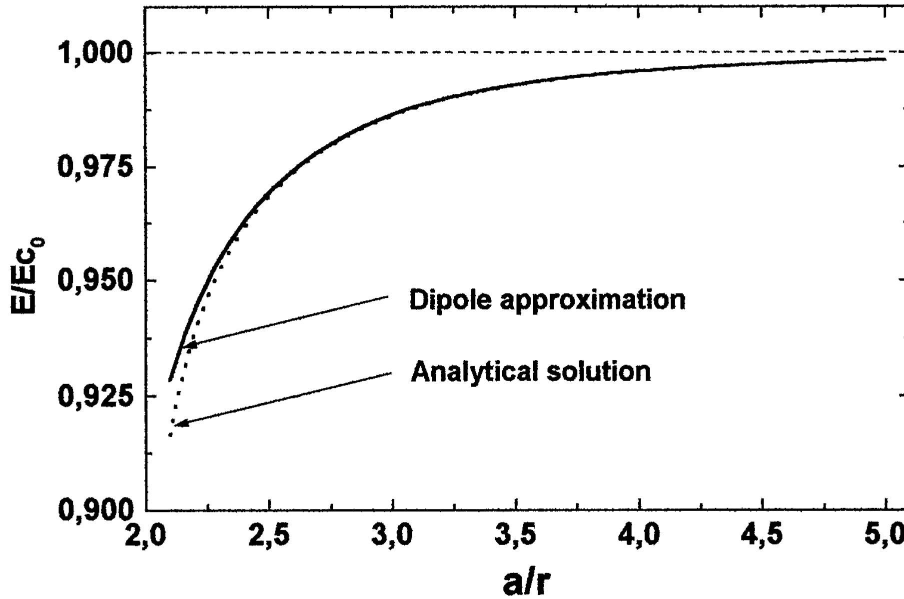

Fig.14. Energy of a system of two spheres (charged and neutral), calculated in the dipole approximation (solid curve) and using the exact analytical formula (dashes curve).

$$E = \int \frac{F(\mathbf{R})^2}{8\pi\varepsilon} d^3\mathbf{R} \ , \tag{4.2}$$

where $F(\mathbf{R})$ is the electric field of the charges Q, q, and $-q$ in vacuum (see Fig. 13a). The integration in Eq.(4.1) was performed numerically by the Monte Carlo method, and the result was compared with the exact analytical solution (see, for example, Ref. 24). The result of this comparison is displayed in Fig. 14. It is evident from the figure that for intersphere distances $a>2r+r/4$ the discrepancy between the first dipole approximation and the exact solution is less than 5%.

To find the total energy E_{ci} of a system of one charged sphere i in an environment of neutral spheres all pairwise dipole corrections to the energy of a charged sphere from each of the neutral spheres were calculated and summed. The dipole-dipole interaction of neutral spheres with one another was neglected, since it is of the next order of smallness. The calculations were performed for a system of 1000 spheres arranged by using the method described above and the results were averaged over all spheres located at distances greater than $L/4$ (L is the size of the system) from the boundaries of the system. In addition, averaging over 100 realizations of random arrangements were performed.

The average charging energy E_C computed in this manner is presented in Fig. 15 as a function of the density of metallic spheres for various values of parameter Δ_{min} of the random arrangement. The dashed curve shows the same dependence for spheres arranged in a simple cubic lattice. In addition, the same figure shows the curves of the rms deviation of E_c from its average value for the same values of Δ_{min}. The inset in Fig. 15 shows as an example the distribution of the charging energies of spheres for a particular case. It is evident, that for sufficiently high densities of the metallic phase the rms deviation of the values of E_C can be a substantial fraction of its averaged value, and together with random potential at the granules [16] it serves as a source of diagonal disorder in the granular medium. It should be noted that this source of disorder has not been considered in previous models of conductivity.

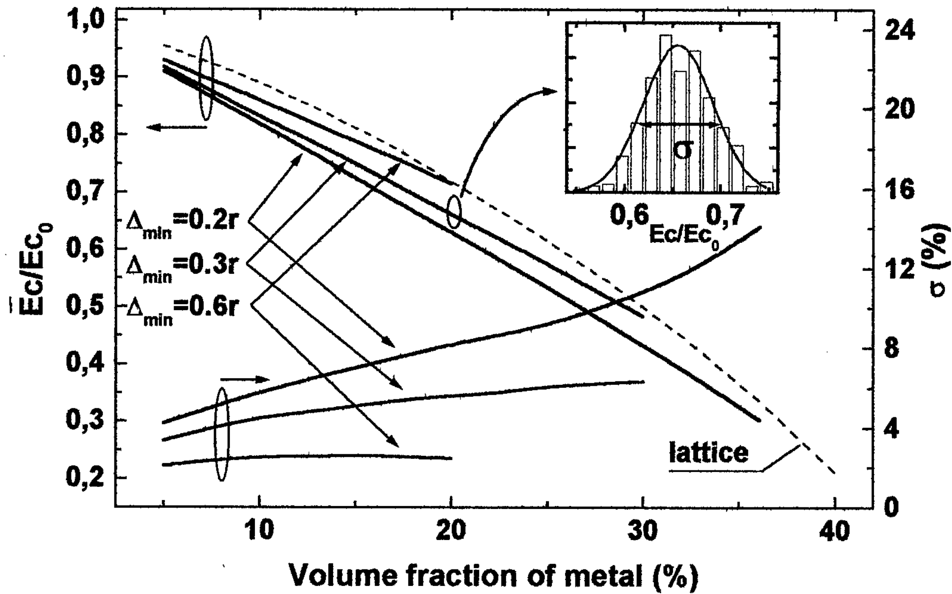

Fig.15. Average charging energy of a sphere and its rms deviation σ as a function of the concentration of the metallic phase for various values of the parameter Δ_{min} of the arrangement and for a cubic lattice of granules (dashed curve).

To calculate in the same approximation the energy of a system of two charged spheres surrounded by neutral spheres, it is necessary to find in the dipole approximation the energy of a system of three spheres, one of which is neutral while the two others are charged, for example, with charges Q and $-Q$. Just as in preceding analysis, we shall use the method of images (Fig. 13b) to take account of the polarization of the spheres, and we shall calculate the energy of such a system using Eq.(4.2), where the integration extends over the entire space outside all three spheres. Subtracting from the energy obtained in this manner the energy of a system consisting of two isolated charged spheres (setting $q_1=0$, $q_2=0$), we obtain a correction due to the polarization of a neutral sphere. To calculate the total energy of a system consisting of two charged spheres in an environment of neutral spheres, we shall sum the corrections due to all neutral spheres, once again neglecting the dipole-dipole interaction of the neutral spheres with one another.

The dependence of the interaction energy of charged spheres, computed in this manner, on the intersphere distance is presented in Fig. 16 for the cases of attraction (charges with different signs) and repulsion (charges with like signs). The curves presented in the figure were averaged just as in the case of the charging energies.

The elements of the inverse matrix C^{-1}_{ij} can be obtained from the charging energies of an arbitrary pair of spheres i and j with charges of same (E^{++}) or different (E^{+-}) signs according to the formulas

$$E^{++}=\left(\frac{C^{-1}_{ii}}{2}+\frac{C^{-1}_{jj}}{2}+C^{-1}_{ij}\right)Q^2, \qquad E^{+-}=\left(\frac{C^{-1}_{ii}}{2}+\frac{C^{-1}_{jj}}{2}-C^{-1}_{ij}\right)Q^2 \qquad (4.3)$$

while the half sum of the energies E^{++} and E^{+-} should equal the sum of the charging energies of the spheres i and j. Thus we can calculate the same quantity - the sum of charging energies

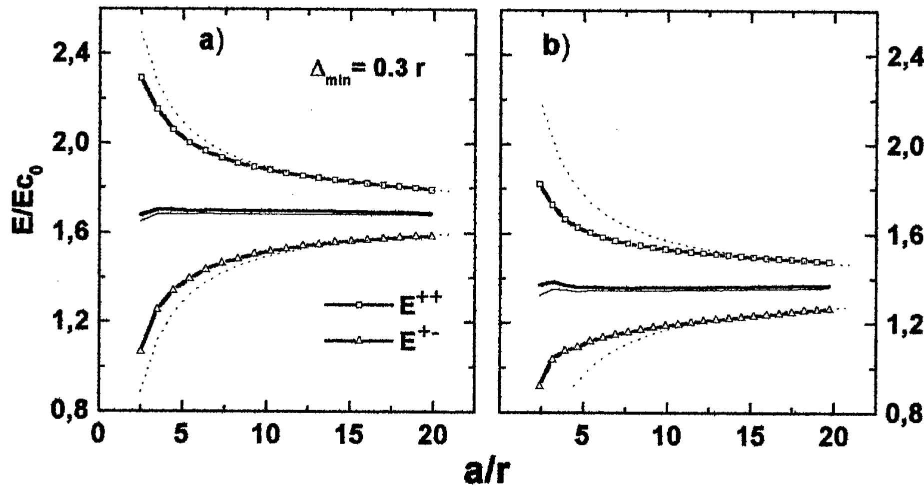

Fig.16. Electrostatic energy of a system of two charged spheres with charges of the same (E^{++}) and different (E^{+-}) signs surrounded by neutral spheres as a function of the intersphere distance for volume concentration of the metallic phase 10% (a) and 20% (b).

(or the diagonal elements of the inverse matrix of capacitance coefficients) - for any pair of spheres by two independent methods. The computational accuracy can be estimated by comparing the results of these calculations. The thick solid lines in Fig. 16 show the half sum $\left(E^{++}+E^{+-}\right)/2$ and the fine lines show the half sum $\left(E_{Ci}+E_{Cj}\right)/2$ of the charging energies. As one can see from the figure, the discrepancy between these curves is ~1% for a 10 vol.% of metal phase and ~2% for a 20 vol.% of metal phase. In order of magnitude this discrepancy is the maximum accuracy that can be obtained in the dipole approximation. As the concentration of spheres increases, this accuracy decreases, because on the average more spheres are located at a short distance from one another, where the error of the dipole approximation is large (see Fig. 14).

The dashed curves in Fig. 16 is the distance depenedence of the average energy of a system of two charged spheres for the case that the electrostatic interaction of these spheres is treated as the interaction of point charges:

$$V_{ij}^{point}=2E_{C0}\left(\frac{\overline{E_C}}{E_{C0}}\pm\frac{1}{a}\right) \tag{4.4}$$

It is evident that for sufficiently large intersphere distances (*a*>*15r*) expression (4.4) describes the computed dependencies quite well. An important feature of the asymptotic expression (4.4) is that the part describing the intersphere interaction does not contain a concentration-dependent effective permittivity, i.e., the Coulomb interaction at large distances drop off just as in a pure dielectric with no metallic inclusions.

4.2. Ground state and one-particle excitation spectrum.

To calculate the ground state of the system the Hamiltonian was written down as:

$$H = \sum_i \varphi_i q_i + \frac{1}{2}\sum_{i,j} C_{ij}^{-1} q_i q_j , \qquad (4.5)$$

where C_{ij}^{-1} is the previously obtained inverse capacitance matrix and φ_i is a so-called "random potential" of granule i presumably associated with surface states at the granules interface or with single metal ions spread in the matrix. This random potential was taken to be uniformly distributed in a given diapason $\Delta\varphi$. The procedure of calculating of the energy spectrum of single-particle excitations was as follows. First, the main state of the system was found, being the state with minimum energy (4.5) with respect to all possible single-electron hops. Then the energies needed to put the additional electron or hole to each particle were calculated. The results are summarized in Fig. 17, where one-particle densities of states for different values of $\Delta\varphi$ are depicted. It can be seen from this figure, that, in case of sufficiently large diagonal disorder, well-pronounced Coulomb-gap occurred at the vicinity of the Fermi-level.

4.3. Calculation of conductivity.

The elementary conductivity of each pair of balls has been calculated as a function of the energy difference between the balls. The probability of electron or hole tunneling from granule i to granule j we write down as [13]:

$$\gamma_{ij} = \gamma_{ij}^0 \exp(-\chi r_{ij}) N(\Delta_i^j) \quad , \qquad (4.6)$$

where γ_{ij}^0 is a constant, χ - tunneling constant, r_{ij} - the distance between granules surfaces and $N(\Delta_i^j)$ - equilibrium Plank phonon distribution:

$$N(\Delta_i^j) = \Delta_i^{j\,2}\left(\exp\left(\frac{\Delta_i^j}{kT}\right) - 1\right)^{-1} \qquad (4.7)$$

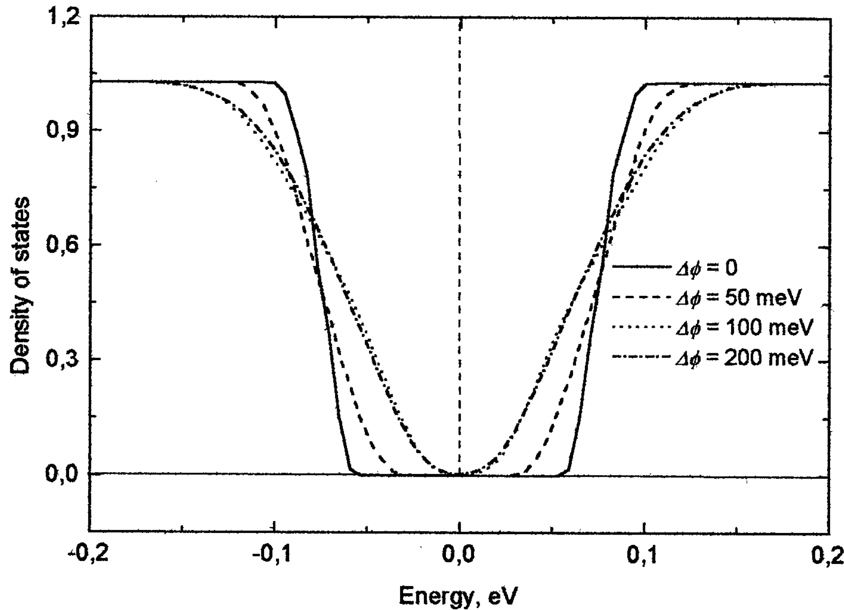

Fig. 17. Simulated one-particle density of states for different values of $\Delta\varphi$.

In these formulas the Δ_i^j stands for the difference between electron or hole energy levels E_i and E_j in granules i and j. From (4.7) the rate of electron jumps $i \to j$ and $j \to i$ can be obtained:

$$\Gamma_{ij} = \gamma_{ij}^0 \exp(-\chi r_{ij}) \int_{E_i'=E_i}^{\infty} \int_{E_j'=E_j}^{\infty} N(\Delta_i^j) f_i (1-f_j) dE_i' dE_j' \qquad \text{(with phonon absorption)}$$

$$\Gamma_{ji} = \gamma_{ij}^0 \exp(-\chi r_{ij}) \int_{E_i'=E_i}^{\infty} \int_{E_j'=E_j}^{\infty} (N(\Delta_i^j)+1) f_j (1-f_i) dE_i' dE_j' \qquad \text{(with phonon emission)}$$

(4.8)

Here f_i and f_j are Fermi occupation numbers of one-particle energy levels in granules i and j. The integrals in (4.8) account for the fact that inside single granule i the electron or hole density of states has a form $\rho(E)=\theta(E-E_i)$ [15].

It can be easily shown that in equilibrium the total rate of electron transfer between two granules $I_{ij}=\Gamma_{ij}-\Gamma_{ji}$ is equal to zero ($\Gamma_{ij}=\Gamma_{ji}=\Gamma_{ij}^0$). But the external field violates this equilibrium. The total current in this case can be expanded in series with respect to the external field, the first term of this series been:

$$I_{ij} = R_{ij}^{-1}(U_i - U_j), \qquad (4.9)$$

where the elementary resistance R_{ij} is $R_{ij} = kT/e\Gamma_{ij}^0$, and U_i , U_j are the potentials of granules i,j.

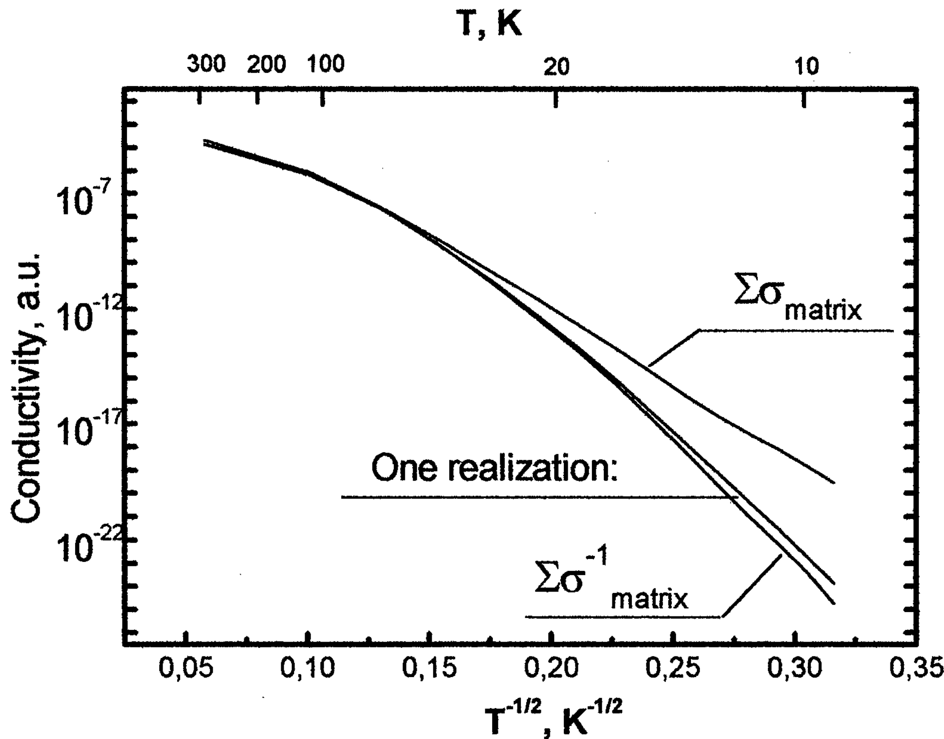

Fig.18. Different ways of averaging of temperature dependencies of conductivity.

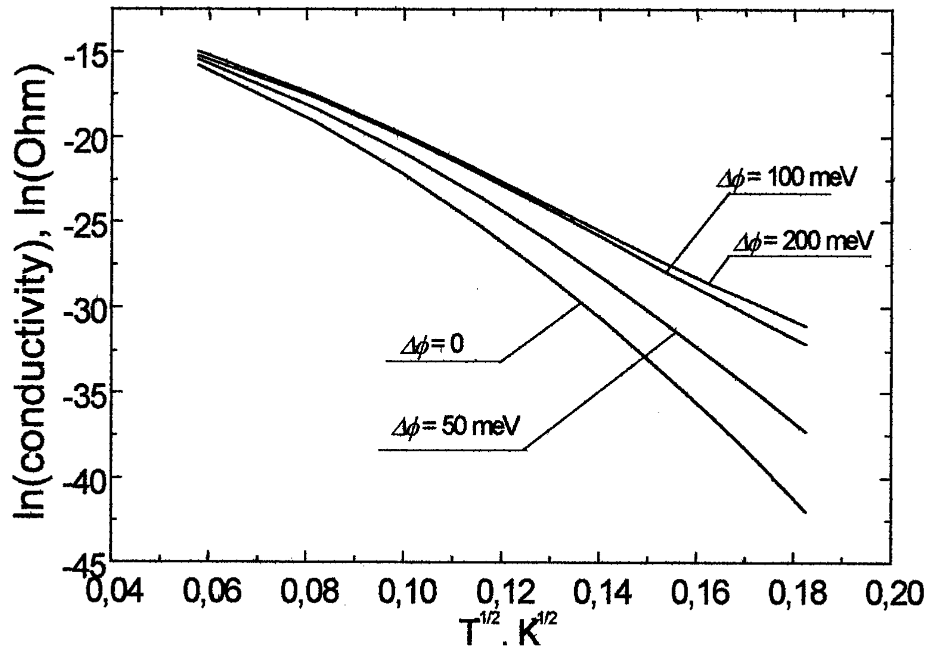

Fig.19. Simulated composite material conductivity as a function of $T^{-1/2}$ for different values of $\Delta\varphi$.

Then, the equivalent network of elementary resistors R_{ij} was built up, including two contact terminals, one grounded and the other biased with given potential. This network was solved in a common way [23].

Finally, the total electrical current was calculated and its temperature dependence was obtained. In general, the result of such calculation depends on the number of balls involved in simulation. To simulate the behavior of bulk samples, the current was calculated in relatively small cell (containing 100-1000 balls) and averaged over large number of random realizations. The averaging was performed as follows: both average value of specific conductivity and average value of specific resistance were calculated, corresponding to the case of parallel cells connection and connection in series, respectively. These two estimates are the low and high limits of specific conductivity of the composite sample containing 10^4 - 10^5 balls. Fig. 18 presents the results of this procedure for the averaging over 100 realizations of cells having 6x6x6 balls. The temperature dependence of conductivity of single cell is also shown in the figure. This result indicates that for the sample containing about 2×10^4 balls, whether the cells are arranged in a wire or in a layer, the conductivity differs several times at room temperature and several orders of magnitude at low temperatures.

Fig. 19 presents the temperature dependencies of conductivity simulated for different values of random potential amplitude $\Delta\varphi$. These calculations were based on OPDOS depicted in Fig. 17 and averaging was performed by summing up the conductivity. The figure shows that bulk conductivity vs. temperature calculated in this way obeys widely observed "$T^{-1/2}$" law at low temperatures only if diagonal disorder is large enough, about 100-200meV. This value is in a good agreement with the estimations of other researches [16]. The deviation from "$T^{-1/2}$" towards higher power of T occurring at higher temperatures which is seen in the figure is also well consistent with the experimental results. We would like to stress that it is Coulomb interaction that is responsible for "$T^{-1/2}$" law. Indeed, the calculations performed without an account for Coulomb interaction result in "$T^{-\alpha}$" dependence, with α about 1/4.

5. Results and discussion.

To perform the quantitative comparison of calculated and experimental results the value of composite material dielectric constant should be known. It would be reasonable to suggest that this value depends on the concentration of the diluted atoms of Cu in the intergranular dielectric. To verify this suggestion, we have performed separate experiment in which the capacitors were fabricated, containing the SiO_2 film with small amount of Cu. The Cu concentration was varied from 0 to 10 vol.%. In this range of concentrations the Cu clusters presumably have not been formed in the film. The dielectric constants were obtained by measuring the capacitance of these samples. These experiments have shown that the dielectric constant of the material increases with Cu concentration from 4 for pure SiO_2 up to 8 for Cu enriched films.

We have used the dielectric constant as a fitting parameter in our calculations. Fig. 20 presents the results of the fitting of experimental temperature dependencies for three composite samples with different metallic phase concentration. The values of dielectric constant delivering the best fits of experimental curves are:

Cu concentration	Dielectric constant
17 vol.%	4.2
27 vol.%	5.9
33 vol.%	7.5

This fit was obtained with the amplitude of random potential $\Delta\varphi$=150meV.

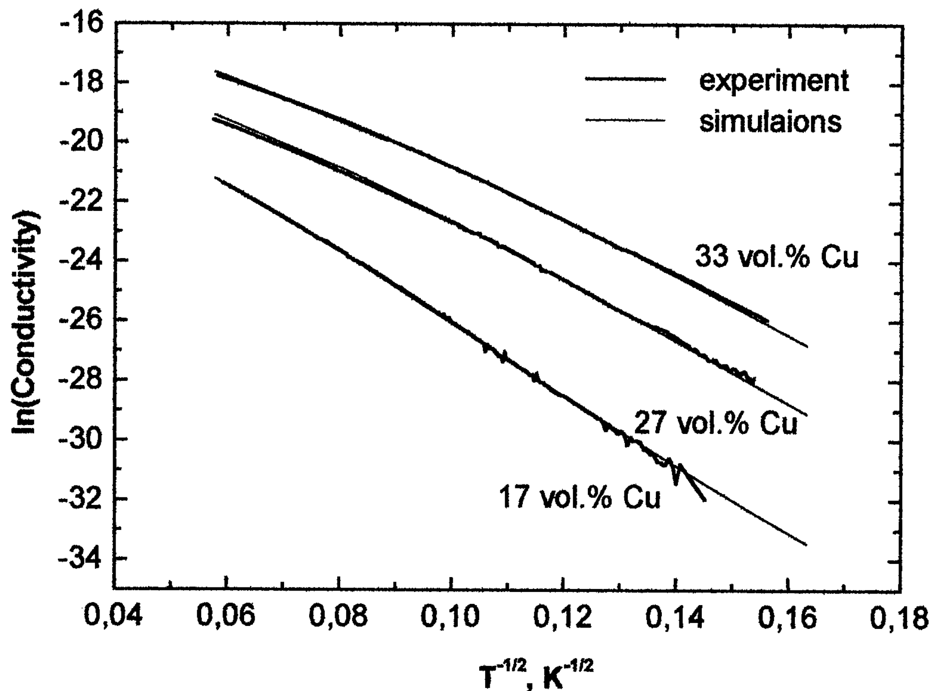

Fig.20. Numerical fitting of experimental temperature dependencies of conductivity of bulk composite films.

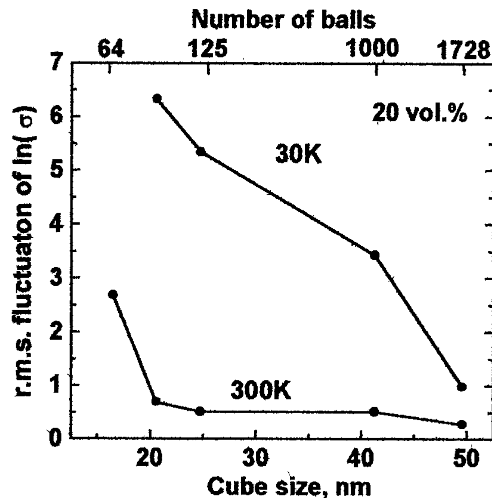

Fig.21. Simulated r.m.s. fluctuations of logarithm of composite sample conductivity vs. sample size.

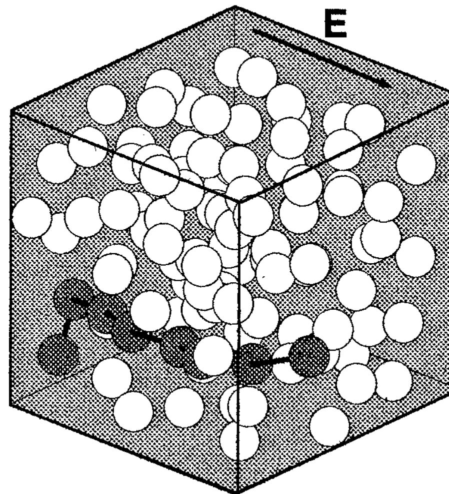

Fig.22. Simulated conducting path carrying 95% of total current. Sample consists of 125 balls, 30K.

This result confirms our initial statement that in the composite films with high Cu concentration certain fraction of Cu remains spread in the form of free-standing atoms.

Let us turn to the temperature dependencies of conductivity of sub-micron samples (see Fig.12). It was outlined that the slope of these dependencies is different for different samples. This difference may be associated with fluctuations of the film composition and contact properties. However, this may also be a manifestation of mesoscopic behavior of these samples arising in systems containing relatively small number of particles.

To clarify this point, we have performed series of calculations of temperature dependencies of low-field conductivity for sets of composite samples having different number of metallic balls. As it was stated in section 4.3, the conductivity varies noticeably from one random realization to another, even when the macroscopic sample characteristics are kept constant. Fig. 21 traces the simulated dependencies of the amplitude of mesoscopic variation of conductivity on the number of particles comprising cubic sample for temperatures 30K and 300K. This figure shows that the amplitude of mesoscopic variation of conductivity sharply decreases as the number of particles increases. For 300K the variation is small for sample size larger than 20nm and such variation could hardly be separated from that associated with technological dispersion of structure parameters. At the same time at 30K the mesoscopic region extends up to cube size about 50nm. Unfortunately, the direct simulations of conductivity variation for sample sizes corresponding to those tested in our experiments are hardly possible due to computer limitations. However, the results in Fig. 21 indicate that for the sample sizes about 100nm the mesoscopic behavior can be observed at low temperatures only.

It would be interesting to note that the results on conductivity variation are sensitive to the degree of disorder in particle positions. This has been found from numerical experiments in which we vary the number of collisions in the procedure defining random ball position (see section 4). So, if in the real structure there is certain inherent correlation in the particles positions (a kind of such correlation was discussed in section 2.3), the mesoscopic limits of conductivity may change. The mesoscopic limit can also be dependent on sample geometry. For example, it obviously should be different for wire-like or planar structures. However, the study of this dependence constitute separate problem not covered in this work.

Fig. 22 illustrates the origin of the mesoscopic behavior. In this figure the dark balls represent the sites at which the current density is maximum in each cross-section normal to the electric field direction (simulation was performed for 30K). As it is seen from the figure, these balls constitute the chain. It was found that this chain carries up to 95% of the total current through the cube. At higher temperatures or in larger samples this chain splits into several branches. In any case, the single chain formation was observed for cubes in which the mesoscopic variation of conductivity is large enough.

6. Conclusions and recommendations.

As we have shown, in mesoscopic regime the low-field conductivity of the system is controlled by the conductivity of the chain constituted by relatively small number of particles. The position of such chain, in principle, could be shifted by electric field of the gate applied perpendicular to main current direction. Switching the conducting path to the different chain should result in change of sample conductivity. However, it would be hardly possible to implement the transistor-like function using this effect. Obviously, this is because initial mesoscopic variations of sample conductivity will be of the same order of magnitude as that resulted from chain switching. We believe that current modulation exceeding mesoscopic variations can be obtained in *nonuniform* structure in which there is a gradient of composition in the direction parallel to the gate field. Such a gradient should stabilize the position of the conducting chain with respect to the gate voltage variation. Contrary to the previous case, in this situation the current can be controlled by changing the potential profile along the chain, without chain switching.

Alternatively, the rearrangement of random potential of metallic particles could be achieved by charging or discharging some of them by means of, for example, carrier injection through tunnel contact. There are some evidences that such quasi-stable charging states may have extremely long relaxation times [25]. The rearrangement of random potential should affect the conducting chains in a similar way the gate potential does. This effect could be used in designing non-volatile memory cells.

The other possibility to implement the transistor (or memory) function should be based on controlling the threshold of high-field regime of mesoscopic conductivity. However, the analysis of conductivity in high-field regime requires further development of our model. This is a serious problem which could be the subject of future studies.

7. Literature cited

1. D.V.Averin and K.K.Likharev, in Mesoscopic Phenomena in Solids ed. by B.Al'tschuler, P.Lee and R.Webb (Elsevier, Amsterdam, 1991), p.169

2. K.K.Likharev, IEEE Trans.Magn. v.23, 1142 (1987)

3. D.Fujita, Z.-C.Dong, H.-Y. Sheng, H.Nejoh, Proc. of the 3rd Int. Symp. on Advanced Physical Fields, Tsukuba, Japan, 18-20 February, 1998, p.340

4. T.Junno, S.-B.Carlsson, Hongqi Xu, L.Montelius, L.Samuelson, Appl. Phys. Letters, v.72 ,p.548 (1998)

5. P.D.Dresselhaus, L.Ji, S.Han, J.E.Lukens, K.K.Likharev, Phys.Rev.Lett., v.72, p.3226 (1994).

6. S.V.Vyshenski, JETP Lett., v.61, 111 (1996)

7. M.E.Raikh, I.M.Ruzin, Mesoscopic Phenomena in Solids, Edited by B.L.Altshuler, P.A.Lee, R.A.Webb, (Elsivier, Amsterdam, 1991), p.315

8. K.Yano, T.Ishii, T.Hashimoto, T.Kobayashi, F.Murai, K.Seki, Int. Electron Devices Meeting IEDM, Washington DC, 1993, p.21.2.1

9. W.Chen, H.Ahmed, K.Nakazoto, Appl.Phys.Lett, v.66(24), 3383 (1995)

10. B.Abeles, P.Sheng, M.D.Coutts, Y.Arie, Adv. Physics, v.24, p.407 (1975)

11. S.A.Gurevich, V.V.Horenko, T.A.Zaraiskaya, L.Yu.Kupriyanov, M.Yu.Kupriyanov, T.N.Vasilevskaya, S.V.Vyshenski, JETP Lett., v.64(10), 736 (1996);

12. V.Ambegaokar, B.I.Halperin, J.S.Langer, Phys. Rev. B, v.4, p.2612 (1971)

13. B.I.Shklovskii, A.L.Efros, Electronic Properties of Doped Semiconductors (Springer, Heidelberg, 1984)

14. A.L.Efros, B.I.Shklovskii, J.Phys. C: Solid State Phys., v.8, p.L49 (1975)

15. J.Klafter, P.Sheng, J.Phys. C, v.17, p.L93 (1984)

16. E. Cuevas, M. Ortuno, J.Ruiz, Phys. Rev. Lett., v. 71, p. 1871 (1993)

17. A.Mobius, M.Richter, B.Drittler, Phys. Rev. B, v.45, p.11568 (1992)

18. A.Alan Middleton, Ned S. Wingreen, Phys. Rev. Letters, v.71, p.3198 (1993)

19. L.D. Landau and E.M. Lifshitz, Course of Theoretical Physics, v.VIII (Pergamon Press, 1960)

20. Ya.B. Zel'dovich, JETP, v.12, p.525 (1942)

21. D.V.Kulikov, Yu.V.Trushin, V.A.Zabelin, S.A.Gurevich, submitted to Proc. SPIE

22. D.A.Zakgeim, I.V.Rozhanskii, S.A.Gurevich, JETP Letters, v.70, p.105 (1999)

23. A.Miller, E.Abrahams, Phys.Rev. v.120, p.745 (1960)

24. V.V.Batygin, I.N.Toptygin, Problems in Electrodynamics (Academic Press, London, 1964)

25. S.A.Gurevich D.A.Zakheim, V.V.Horenko, T.A.Zaraiskaya, E.M.Tanklevskaya, Proc. of Int. Symp. "Nanostructures: Physics and Technology", St.-Petersburg, 23-27 June 1997, p.474.